Modification of the Properties of Al$_2$O$_3$/TZ-3YS Thermal Barrier Coating by the Addition of Silicon Carbide Particles and Fructose

Amparo Borrell [1,*] , **Pablo Carpio** [1] , **Maria Dolores Salvador** [1] , **David Busquets Mataix** [1] , **Víctor Carnicer** [2] and **María José Orts Tarí** [2]

[1] Instituto de Tecnología de Materiales (ITM), Universitat Politècnica de València (UPV), Camino de Vera s/n, 46022 Valencia, Spain; pabcarco@upv.es (P.C.); dsalva@mcm.upv.es (M.D.S.); dbusquets@mcm.upv.es (D.B.M.)

[2] Instituto de Tecnología Cerámica (ITC), Universitat Jaume I (UJI), Av. Sos Baynat, 12006 Castellón, Spain; victor.carnicer@itc.uji.es (V.C.); mariajose.orts@itc.uji.es (M.J.O.T.)

* Correspondence: aborrell@upv.es; Tel.: +34-963877000

Abstract: Al$_2$O$_3$/TZ-3YS coatings developed by suspension plasma spraying were studied in the present work. Mechanical and thermal characterization was realized to evaluate the suitability of thermal barrier coatings. In addition, SiC particle reinforcement was evaluated for its effect on the mechanical properties of the coating. The problem with SiC reinforcement is its high melting point that causes a large amount of unmolten material to be deposited on the coating. One possible solution followed in the present study consists of including fructose as an additive in order to modify the suspension characteristics. The results conclude that the use of fructose as an additive increases the mechanical and thermal properties (from 1.0 to 1.6 W/m·K), since the microstructure is modified, and results in a lower porosity (17%) compared to the SiC coating (25%).

Keywords: SPS process; SiC deposition; TBCs; coating properties

1. Introduction

In recent decades, ceramic coatings developed by atmospheric plasma spraying (APS) have been widely studied. In the APS technique, the powder is injected inside the plasma plume, where the material is molten and accelerated for adherence onto the substrate. One of the possible APS applications is to obtain thermal barrier coatings (TBCs) that protect the metallic substrate against extremely hot environments [1]. These coatings are conventionally made of yttria-stabilized tetragonal zirconia (Y-TZP) because of its low thermal conductivity and good mechanical behavior at high temperatures [2]. However, Y-TZP coatings show a low stabilization at high temperature. Therefore, the eutectic mixture Al$_2$O$_3$/Y-TZP has been proposed as an alternative composition. Previous studies have demonstrated that Al$_2$O$_3$/Y-TZP coatings exhibit an enhanced thermodynamic stabilization, mechanical properties, and thermal fatigue resistance [3,4].

The APS technique shows some limitations, i.e., obtaining a microstructure with small features, as fine particles cannot be injected inside the plasma plume. One alternative is the suspension plasma spraying (SPS) technique that employs injecting suspensions instead of powders into the plasma torch [5,6]. In this case, the liquid is fragmented in small droplets, and the solvent must evaporate before the solid can be molten and adhered onto the substrate. The TBC developed by SPS exhibits lower thermal conductivity, and this technique does not worsen the mechanical properties [3,6]. However, the SPS technique has some inconveniences, such as low deposition efficiency and difficulty to melt refractory materials. When aqueous suspensions are used, one possibility to improve the feedstock is to increase the solid loading due to high heat requirements to evaporate the water [4]. An alternative route involves the use of additives like fructose, which reduces the viscosity

and surface tension so the formed droplet inside the plasma plume is smaller, and it eases solvent evaporation and solid melting [7].

In the present work, alumina–zirconia coatings developed by SPS are studied. In order to improve the characteristics of these coatings, the possibility of reinforcing the composition with silicon carbide particles (SiC) is evaluated. SiC exhibits two functions: mechanical reinforcement and self-healing. The self-healing effect by oxidation of SiC can increase the TBC's lifetime, but it will be extensively studied in future work [7,8]. The problem of adding SiC is the capacity heat. To solve this problem, suspensions with high solid-loading were prepared, and new additives, like fructose, were evaluated [7]. In a previous work, it was found that fructose modified the microstructure of the coatings. Therefore, the goal of the present study is to analyze how this affects the mechanical and thermal properties of the coatings.

2. Experimental Procedure

2.1. Coating Development

Multicomponent suspensions with a 20 vol.% (around 40 wt.%) solid loading were prepared as feedstock. The different components were mixed in deionized water with dispersant: polyacrylic acid (PAA; Duramax TM D-3005, Rohm & Haas, Philadelphia, PA, USA) and a synthetic polyelectrolyte (PKV, Produkt KV5088, Zschimmer-Schwarz, Germany). The components were as follows: α-alumina (CT3000SG, Almatis, Ludwigshafen, Germany), tetragonal zirconia polycrystal doped with 3 mol% Y_2O_3 (TZ-3YS, Tosoh Co., Tokyo, Japan), and α-silicon carbide (IF-15, Hermann C. Starck, Goslar, Germany). The average particle sizes (d_{50}) of α-Al_2O_3, TZ-3YS and α-SiC were 0.5, 0.4 and 0.6 μm, respectively. More details about the raw materials and suspension preparation are described in previous work [7,9]. A total of three suspensions were prepared: Al_2O_3/TZ-3YS suspension in a eutectic ratio (60/40 wt.%); Al_2O_3/TZ-3YS suspension with a 15 wt.% SiC that acts as reinforcement agent; and Al_2O_3/TZ-3YS suspension with SiC using the same ratio but adding 20 wt.% D-fructose (AppliChem GmbH, Darmstadt, Germany) that acts as an additive to modify the suspension rheology and surface tension, according to a previous work by the authors [7].

The three prepared feedstocks were deposited onto a metallic substrate by a plasma torch (F4-MB, Oerlikon Metco, Switzerland) controlled with a robot (IRB, ABB, Switzerland). Before spraying, the metallic substrates were sandblasted with corundum at a constant pressure of 4.2 bars and cleaned in ethanol and an ultrasonic bath. AISI type 304 stainless steel was used as substrate, which was grit-blasted using black corundum until a surface roughness (Ra) of 2.2 $\pm$ 0.1 μm was reached and then cleaned with ethanol. A NiCoCrAlTaY superalloy (Amdry 997, Oerlikon-Metco, Salzgitter, Germany) was deposited as a bond coat by atmospheric plasma spraying [7]. The deposition parameters, which are shown in Table 1, were selected from previous research [10].

Table 1. Main spraying parameters.

Ar (slpm) *	H$_2$ (slpm)	Electric Intensity (A)	Scan Speed (m/s)	Suspension Feed Rate (mm^3/s)	Specimen Holder Speed (m/s)	Distance (mm)
37	8	700	1.25	450	0.72	40

* slpm: standard liter per minute.

2.2. Microstructural Analysis

The coating microstructure was observed in surface and cross-section by field-emission scanning electron microscope (FE-SEM, S-4800, Hitachi, Tokyo, Japan). The cross-sectional surface was metallographically prepared by mounting in an epoxy resin and was subsequently polished with diamond. In addition, FE-SEM was connected to EDX (Energy-Dispersive X-ray spectroscopy) equipment (Oxford Instruments, Abingdon, UK) to carry out microanalysis of different features observed in the microstructure.

Moreover, porosity and the number of unmolten/resolidified zones were quantified by image analysis software (Image-Pro Plus) from 20 cross-section FE-SEM images at 500× magnification. Porosity was quantified by thresholding, while the unmolten zones were manually identified.

The crystalline phases were determined by X-ray diffraction (XRD, AXS D5005, Bruker, Karlsruhe, Germany) with Cu Kα radiation (λ = 1.54183 Å). The measurements were performed in the 20–80 range, and the step size and time of reading were 0.021 and 0.3 s, respectively.

2.3. Mechanical Characterisation

The mechanical behavior of the coatings was evaluated by measuring hardness and elastic modulus with a nanoindentation test (G-200 nanoindenter, Agilent Technologies, Cheadle, UK). A diamond Berkovich tip previously calibrated on silica reference material was used to make the measurements. The stiffness was calculated by a continuous stiffness measurement (CSM) mode set at 2 nm harmonic oscillation amplitude and 4 Hz oscillation frequency. CSM mode allows a continuous measurement of basic mechanical properties during loading with the indenter [11]. Indentations were performed on the polished sample at the cross-sectional view and at a constant 2000 nm depth. Diverse locations in the coating were selected to analyze the mechanical behavior. The location of the test was guided by an optical microscope included in the nanoindenter machine.

The adhesion strength between layers was also determined by the pull-off test using an automatic adhesion tester (posiTest AT-100, DeFelsko, Ogdensburg, NY, USA). The test consists of several metallic disks (dolly) that are glued on the coating surface by epoxy glue (Araldite 2000, Hunstman, The Woodlands, TX, USA), and an electronically controlled hydraulic pump applies a continuous pull-off pressure until the coating is peeled-off. The glued coating beyond the dolly is released and subsequent observation serves to corroborate how the failure was produced (adhesive failure between layers or cohesive failure inside one layer). Then, adhesion strength is calculated from the ultimate force registered by the instrument.

2.4. Thermal Characterisation

Thermal diffusivity was determined with xenon flash lamp equipment (LFA467 HT Hyperflash, Netzsch-Gerätebau GmbH, Selb, Germany) at different temperatures of up to 1000 °C. A thin layer of graphite was deposited on both sides of the sample to improve the signal, and an argon atmosphere was used to prevent oxidation of the sample at high temperatures.

Then, thermal conductivity was calculated using Proteus analysis software (Netzsch-Gerätebau GmbH, Selb, Germany) from the measured diffusivity of the complete system (substrate, bond coat, and coating), specific heat (Cp), density, and diffusivity. Specific heat was obtained from the literature, while density (related by the porosity) and thickness were experimentally calculated from image analysis. The three-layer model was used to correct the pulse emitted by the flash lamp and heat loss between the different layers of the coating [12].

3. Results

3.1. Microstructure

Figure 1 shows the topography of the different coatings. It can be observed that the coatings are formed by fine particles, but differences were observed between them. Coatings A (Al_2O_3/TZ-3YS) and B (Al_2O_3/TZ-3YS/SiC) are flattened with some mounds, the morphology commonly observed in coatings formed by lamellas or splats. However, coating C (Al_2O_3/TZ-3YS/SiC + fructose) displays a cauliflower-type microstructure, which is common in columnar-type coatings [13].
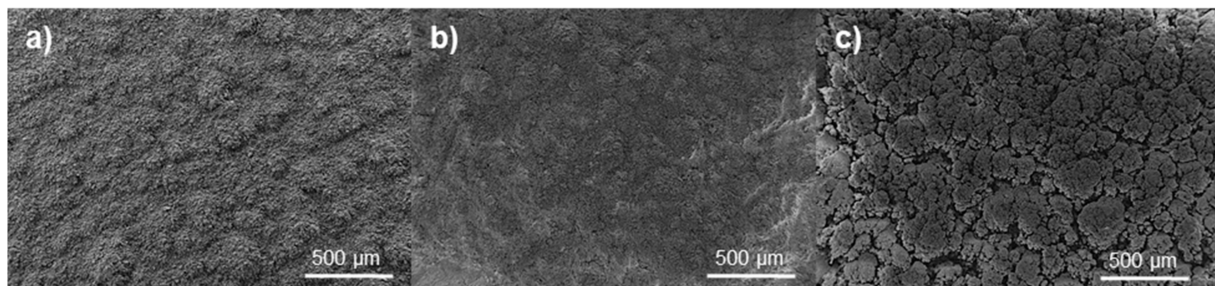
Figure 1. Surface micrographs of different suspension plasma spraying (SPS) coatings: (**a**) Al_2O_3/TZ-3YS; (**b**) SiC-reinforced Al_2O_3/TZ-3YS; (**c**) SiC-reinforced Al_2O_3/TZ-3YS with fructose.

The cross-section of the coatings (Figure 2) confirms the observations made in Figure 1. Coatings A (Al_2O_3/TZ-3YS) and B (Al_2O_3/TZ-3YS/SiC) show a lamellar microstructure formed by molten splats and unmolten zones. The unmolten zones can be caused by both unmolten particles imbibed inside the molten matrix and the full melting of fine particles and subsequent solidification [6]. The main characteristic of these coatings compared with the other two-zone microstructure coatings typical in SPS and SPPS coatings [14] is based on the fact that, in this case, unmolten zones present an elongated morphology, and they are homogeneously distributed between molten splats so that the coating is formed by molten and unmolten lamellae layered together [7].
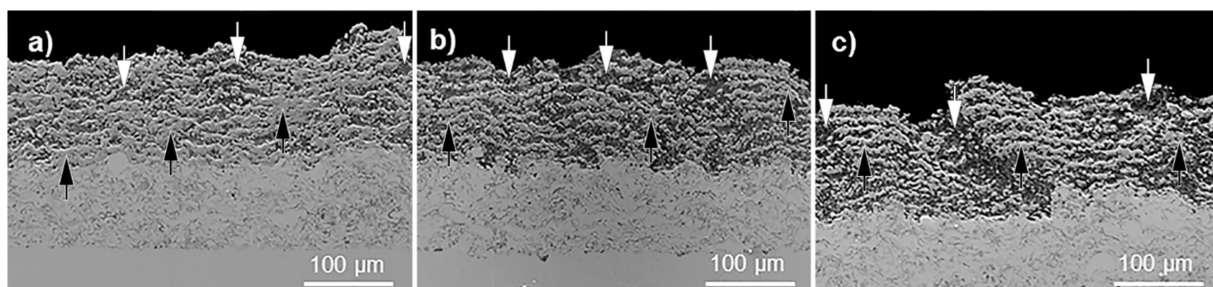

Figure 2. Cross-section micrographs of different SPS coatings: (**a**) Al_2O_3/TZ-3YS; (**b**) SiC-reinforced Al_2O_3/TZ-3YS; (**c**) SiC-reinforced Al_2O_3/TZ-3YS with fructose. The different zones of the coating are marked with arrows: white arrows indicate unmolten/resolidified zones, and black arrows indicate fused zones.

In addition, the cross-section of the C (Al_2O_3/TZ-3YS/SiC + fructose) coating has an irregular structure when compared to the A (Al_2O_3/TZ-3YS) and B (Al_2O_3/TZ-3YS/SiC) coatings, which have a block or laminate structure. These irregularities confirm the cauliflowers seen on the surface and suggest that the addition of fructose has a positive impact on modifying the droplets sprayed in the plasma torch, by decreasing the surface tension, as observed by Carnicer et al. [7]. Ganvir et al. [15] observed that the use of ethanol, whose surface tension is much lower than that of water, allows the formation of well-defined columnar structures because smaller, homogeneous drops, which are dragged more easily by the plasma flow, can be sprayed. However, it is important to take into account the high flashpoint of ethanol. Therefore, it is preferable to use water as the solvent.

Microstructural differences are reflected in the porosity values, which are shown in Table 2. The addition of SiC particles increased the porosity and the unmolten zones, as can be corroborated by Figure 2, because the SiC decomposition point is higher than that of the other oxides employed. This indicates that the power in the plasma plume is insufficient for complete melting of the particles. However, the addition of fructose did not significantly change the porosity value, but it did change its position. The porosity and unmolten zone ratio are similar between both coatings with SiC reinforcement (with and without fructose), but they showed a tendency towards the columnar structure when fructose was added. This tendency is caused by the lower surface tension that favors the formation of smaller

droplets during fragmentation [7,15]. In addition, the degradation temperature of fructose is around 180 °C, which is a higher temperature than that of water evaporation but much lower than that of the plasma plume. This could provide energy to the plasma torch during oxidation of the saccharide, similarly to the way energy is provided during the degradation of ethanol in suspensions with this solvent [16].

Table 2. Porosity and unmolten/resolidified zones ratio in the coatings.

Properties	Al_2O_3/TZ-3YS	Al_2O_3/TZ-3YS/SiC	Al_2O_3/TZ-3YS/SiC + Fructose
Porosity (%)	13 ± 1	25 ± 3	17 ± 8
Unmolten/resolidified zones ratio (%)	28 ± 5	53 ± 6	54 ± 4

The chemical composition of the coatings is barely homogeneous. Figure 3 displays an unmolten zone embedded in a molten matrix, in which dark and bright particles are observed to correspond to Al_2O_3 and TZ-3YS particles, respectively. On the other hand, splats with different composition were also observed. The most extended splats, with a grey color, correspond to the eutectic mixture Al_2O_3/TZ-3YS, while darker or lighter zones consist of splats richer in Al_2O_3 or in TZ-3YS. These findings suggest that the time inside the plume is not enough for the whole mixture to reach the eutectic temperature, and splats with different composition were observed.
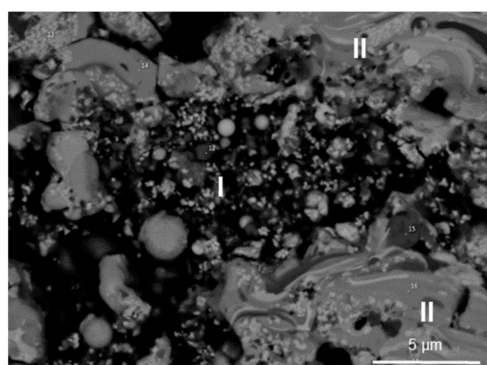

Figure 3. FE-SEM micrograph of Al_2O_3/TZ-3YS coating at 2500× backscattering mode. Unmolten and molten zones are marked by I and II, respectively. Black and white particles inside the unmolten zone correspond to Al_2O_3 and SiC, respectively.

Moreover, SiC particles can be observed, both in unmolten zones and imbibed inside the molten matrix, when they are included in the feedstock (Figure 4). It is important to remark that SiC was only identified as particles and not in the splat composition, showing that SiC is not molten, at least not in an important amount. This is comprehensible since its melting point is considerably higher, and it cannot form a eutectic with Al_2O_3 or TZ-3YS. Most SiC particles were imbibed inside the coating, but some SiC could not be retained since around 11 wt.% Si (corresponding to 10 wt.% SiC compared to the started 15 wt.%) was quantified by EDX in the coatings (with and without fructose).

Figure 5 displays the XRD pattern of the produced coatings. α-Al_2O_3, tetragonal ZrO_2, and α-SiC were successfully identified, and, therefore, Al, Zr, and Si previously observed by EDX mainly correspond to these phases, respectively. The Al_2O_3/TZ-3YS coating contains only α-Al_2O_3 and tetragonal ZrO_2, while no significant differences were observed among the Al_2O_3/TZ-3YS/SiC coatings (with and without fructose).
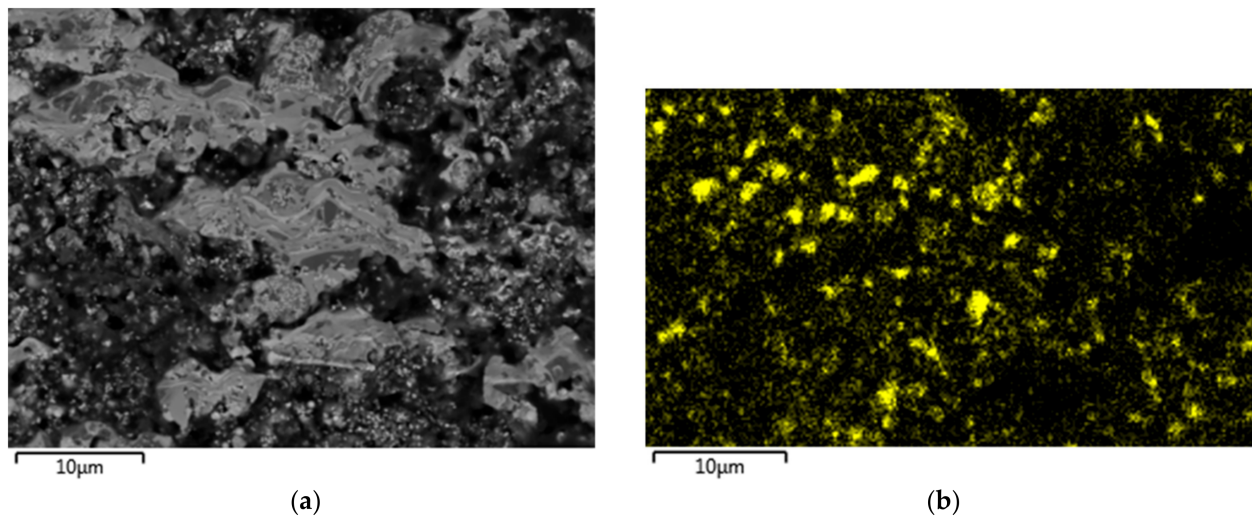
Figure 4. Micrograph of Al_2O_3/TZ-3YS/SiC with fructose coating at 2500×: (**a**) micrograph at backscattering mode; (**b**) mapping performed by EDX where Si is marked.
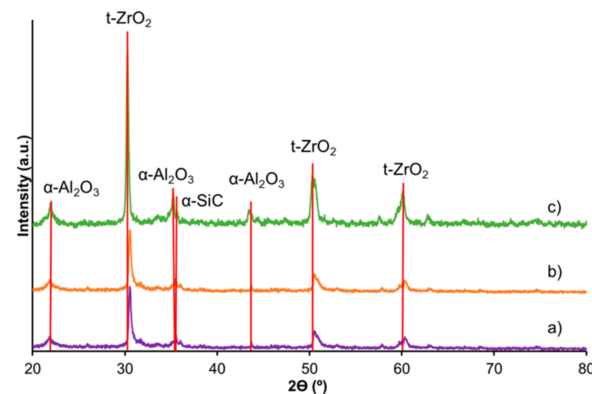

Figure 5. XRD pattern of Al_2O_3/TZ-3YS coatings: (**a**) without reinforcement; (**b**) SiC-reinforced; (**c**) with fructose and SiC-reinforced.

3.2. Mechanical Properties

The mechanical behavior of the coatings was evaluated in terms of hardness and modulus curves at different penetrations, as shown in Figure 6. Molten and unmolten/resolidified zones of the coatings were analyzed, and it was corroborated that their behavior is different. Hardness and modulus values at low penetration (smaller than 50 nm) are unrepresentative, as sample roughness, impurities in the nanoindenter, or the elastic behavior of the materials (both nanoindenter and coating) are crucial. A maximum in hardness and modulus was observed at 50–100 nm, although this value was higher in the molten zone because of its low porosity. Then the values decreased, although they were more pronounced in the unmolten/resolidified zones. The reason is that the material crumbles when a load is applied. The hardness and modulus in molten zones also decrease because the effect of adjacent zones is more pronounced at higher depths. In fact, a minimum was observed in unmolten/resolidified zones at around 400 nm, and then the curve slightly rose until it matched the curve corresponding to the molten zone because of the adjacent effect. These effects were observed at lower depths in hardness than in modulus because the influence of the modulus is higher.
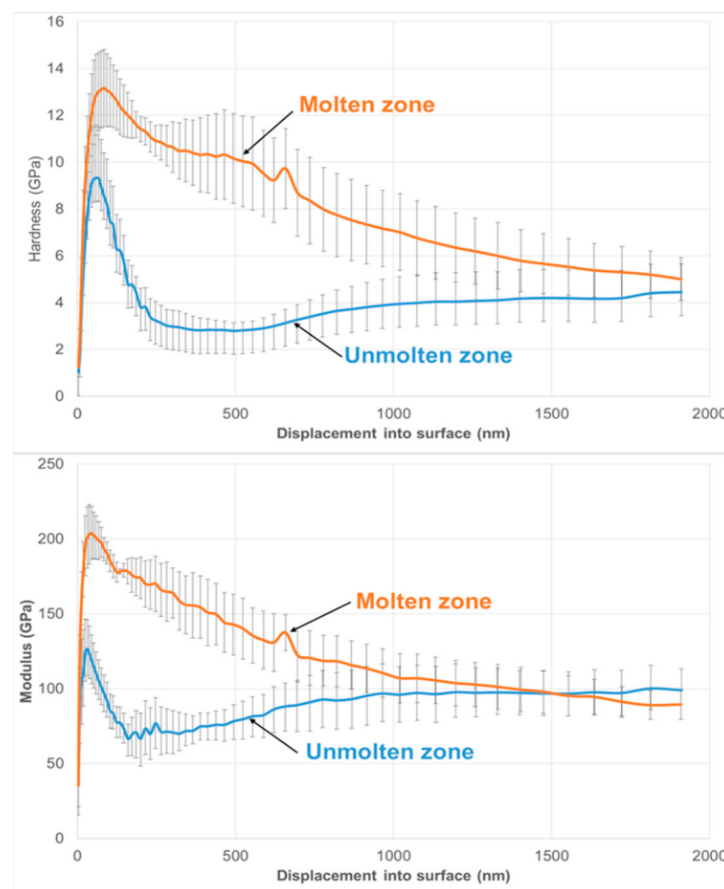
Figure 6. Hardness and modulus at different penetration depths of the Al_2O_3/TZ-3YS coating in different regions.

The behavior described above is common in all coatings, but differences were observed between them, as shown in Figure 7. SiC can entail a reinforcement depending on the coating microstructure. The Al_2O_3/TZ-3YS/SiC coating without fructose displayed a poor value of hardness and modulus, being especially low in unmolten/resolidified zones. These poor mechanical properties are due to its excessively high porosity; therefore, SiC particles cannot provide reinforcement. However, the reinforcement effect was observed in coatings with fructose. In this case, the hardness peak was even higher compared to that of the coating without SiC (Al_2O_3/Y-TZP), although the reinforcement effect was less noticeable at higher depths. Coatings with fructose display a lower porosity, although their unmolten/resolidified zone ratio is high. This means that unmolten zones on coatings with fructose are quite dense, and this fact unsubstantially worsens the properties. Hence, two coatings with the same composition show a different mechanical behavior due to their microstructures.

Figure 8 shows the adhesion strength value of the coatings as well as the detached coating determined by the pull-off test. The failure originated between the bond coat and top coat in all cases, as this is common in TBCs, but the adherence value was quite poor in coatings with SiC. Unmolten/resolidified zones were retained between the bond coat and the molten matrix, and these zones could not act as bonding, as can be observed in Figure 9. For this reason, SiC coatings with a high content of unmelted/resolidified zones show inadequate adhesion. This problem caused by the microstructure can be solved with a new design, such as multilayer or functionally graded coatings, where a layer with higher adherence (layer without SiC) is deposited between the bond coat and the layer with SiC.
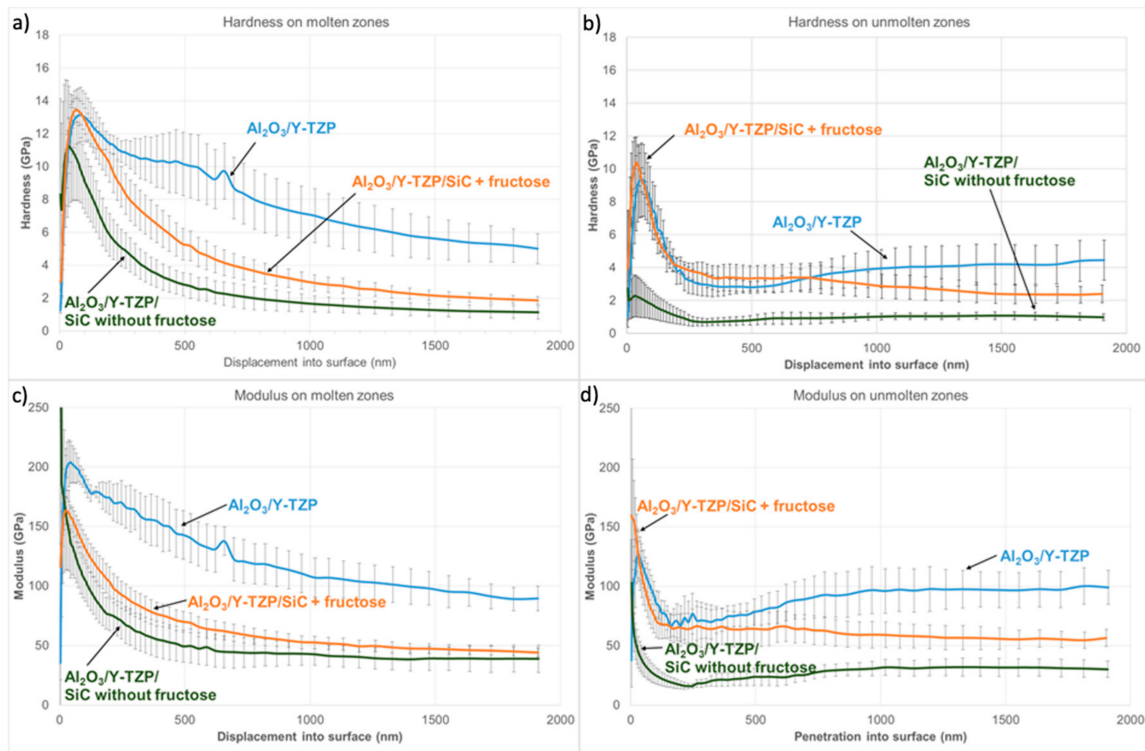
Figure 7. Hardness and modulus at different penetration depths of different samples: (**a**,**c**) on molten zones; (**b**,**d**) on unmolten zones.
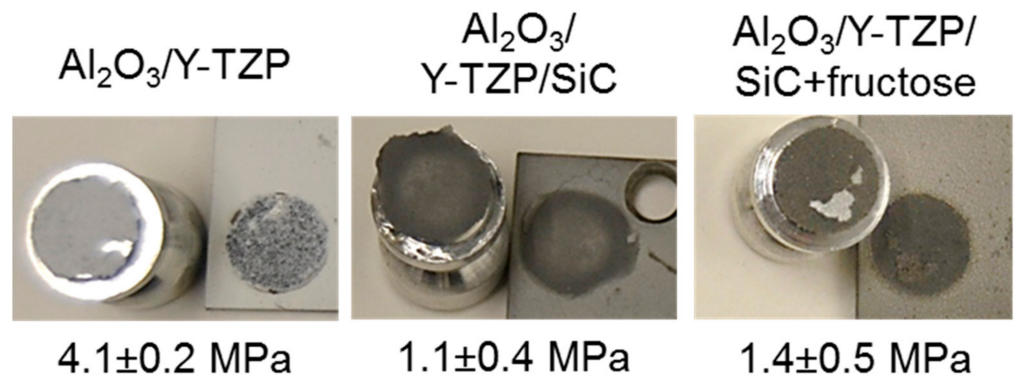

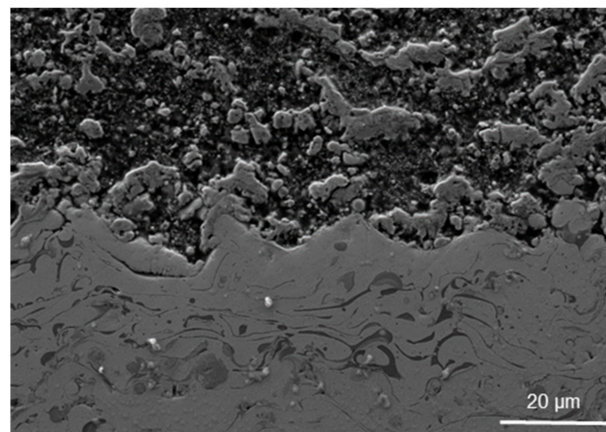**Figure 8.** Tested samples by pull-off and their adherence values.

Figure 9. Bond coat/top coat interface of Al_2O_3/TZ-3YS coating at 5000×.

3.3. Thermal Conductivity

The developed Al_2O_3/TZ-3YS coatings show thermal conductivity similar to or even lower than that of the conventional TBC found in the literature, despite Al_2O_3 showing higher conductivity than Y-TZP [17] (Figure 10). This may be due to the high porosity of the coating. Thus, Al_2O_3/TZ-3YS represents a good alternative when designing TBCs since it exhibits improved mechanical properties and similar thermal conductivity. The reason for this is that the microstructure—specifically, the porosity and its distribution—improves the thermal insulation in coatings reinforced with SiC.
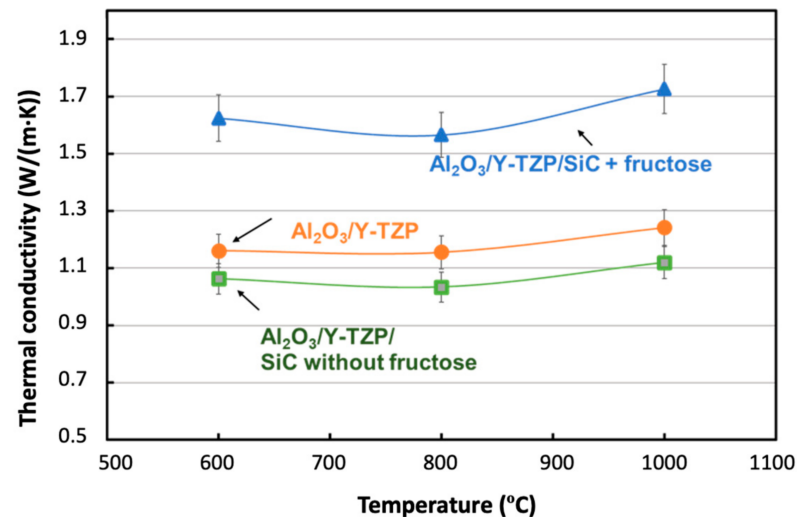

Figure 10. Thermal conductivity of the coatings at different temperatures.

The coating with fructose displayed a slightly higher thermal conductivity than those without fructose despite having similar porosity. Hence, porosity distribution is also important in thermal insulation, as has been reported in the literature [18]. Pores distributed in columns, as is exhibited in coatings from feedstocks with fructose, cannot act as a thermal barrier, and they can even enable heat transmission by convection [18]. It is important to note that the thermal conductivity rose slightly, and it was around the conventional values for TBCs. However, the columnar coating has other advantages, such as the improvement in thermal fatigue resistance [19].

4. Conclusions

Al_2O_3/TZ-3YS coatings can been reinforced with SiC particles. However, the effect of this reinforcement depends on the way SiC is introduced inside the coating. For this reason, the addition of fructose together with SiC was evaluated in the present work in order to study its influence on the coating microstructure.

Adding SiC considerably increases the number of unmolten/resolidified zones since plasma power is insufficient to melt the SiC particles. Adding fructose causes a microstructural modification that affects the coating properties. The addition of SiC particles causes a worsening of mechanical properties because of the high porosity and the number of unmelted zones. Nevertheless, this negative effect is mitigated when fructose is also added, as SiC particles reinforce the unmolten zones in this case.

Unfortunately, a slight increase in thermal conductivity occurs since fructose provokes a change in porosity orientation, but it can be beneficial for other properties, such as thermal fatigue resistance.

In conclusion, it is important to consider the microstructure, as well as the composition, to predict the mechanical and thermal properties in a coating. SiC particles, despite their higher hardness, cannot provide reinforcement if they cause porosity. Therefore, this study has shown that one possible way to solve the SiC melting problem is with the addition of fructose.

Author Contributions: Conceptualization, M.J.O.T.; data curation, P.C.; formal analysis, D.B.M. and V.C.; funding acquisition, M.D.S.; investigation, A.B. and P.C.; methodology, A.B. and V.C.; project administration, M.D.S. and D.B.M.; resources, M.D.S.; supervision, M.J.O.T.; writing—original draft, P.C. and M.J.O.T.; writing—review & editing, A.B. and D.B.M. All authors have read and agreed to the published version of the manuscript.

Institutional Review Board Statement: Not applicable.

Informed Consent Statement: Not applicable.

Data Availability Statement: Data sharing not applicable.

Conflicts of Interest: The authors declare no conflict of interest.

References

1. Sahith, M.S.; Giridhara, G.; Kumar, R.S. Development and analysis of thermal barrier coatings on gas turbine blades—A review. *Mater. Today Proc.* **2018**, *5*, 2746–2751. [CrossRef]
2. Lavasani, H.Q.; Valefi, Z.; Ehsani, N.; Masoule, S.T. Comparison of the effect of sintering on the microstructure, micro hardness and phase composition of conventional and nanostructured YSZ TBCs. *Ceram. Int.* **2017**, *43*, 12497–12504. [CrossRef]
3. Tarasi, F.; Medraj, M.; Dolatabadi, A.; Oberste-Berghaus, J.; Moreau, C. Effective parameters in axial injection suspension plasma spray process of alumina-zirconia ceramics. *J. Therm. Spray Technol.* **2008**, *17*, 685–691. [CrossRef]
4. Carpio, P.; Salvador, M.; Borrell, A.; Sánchez, E.; Moreno, R. Alumina-zirconia coatings obtained by suspension plasma spraying from highly concentrated aqueous suspensions. *Surf. Coat. Technol.* **2016**, *307*, 713–719. [CrossRef]
5. Pawlowski, L. Suspension and solution thermal spray coatings. *Surf. Coat. Technol.* **2009**, *203*, 2807–2829. [CrossRef]
6. Fauchais, P.; Joulia, A.; Goutier, S.; Chazelas, C.; Vardelle, M.; Rossignol, S. Suspension and solution plasma spraying. *J. Phys. D Appl. Phys.* **2013**, *46*. [CrossRef]
7. Carnicer, V.; Martinez-Julian, F.; Orts, M.; Sánchez, E.; Moreno, R. Effect of fructose-containing feedstocks on the microstructure of multicomponent coatings deposited by suspension plasma spraying. *J. Eur. Ceram. Soc.* **2019**, *39*, 3433–3441. [CrossRef]
8. Koch, D.; Mauer, G.; Vaßen, R. Manufacturing of composite coatings by atmospheric plasma spraying using different feed-stock materials as YSZ and MoSi$_2$. *J. Therm. Spray Technol.* **2017**, *26*, 708–716. [CrossRef]
9. Carnicer, V.; Alcazar, C.; Sánchez, E.; Moreno, R. Aqueous suspension processing of multicomponent submicronic Y-TZP/Al$_2$O$_3$/SiC particles for suspension plasma spraying. *J. Eur. Ceram. Soc.* **2018**, *38*, 2430–2439. [CrossRef]
10. Carnicer, V.; Orts, M.J.; Moreno, R.; Sanchéz, E. Microstructure assessment of suspension plasma spraying coatings from multicomponent submicronic Y-TZP/Al$_2$O$_3$/SiC particles. *Ceram. Int.* **2018**, *44*, 12014–12020. [CrossRef]
11. Carpio, P.; Bannier, E.; Salvador, M.D.; Borrell, A.; Moreno, R.; Sánchez, E. Effect of particle size distribution of suspension feedstock on the microstructure and mechanical properties of suspension plasma spraying YSZ coatings. *Surf. Coat. Technol.* **2015**, *268*, 293–297. [CrossRef]
12. Sokołowski, P.; Łatka, L.; Pawłowski, L.; Ambroziak, A.; Kozerski, S.; Nait-Ali, B. Characterization of microstructure and thermal properties of YCSZ coatings obtained by suspension plasma spraying. *Surf. Coat. Technol.* **2015**, *268*, 147–152. [CrossRef]
13. VanEvery, K.; Krane, M.J.M.; Trice, R.W. Parametric study of suspension plasma spray processing parameters on coating microstructures manufactured from nanoscale yttria-stabilized zirconia. *Surf. Coat. Technol.* **2012**, *206*, 2464–2473. [CrossRef]
14. Kozerski, S.; Łatka, L.; Pawlowski, L.; Cernuschi, F.; Petit, F.; Pierlot, C.; Podlesak, H.; Laval, J.P. Preliminary study on suspension plasma sprayed ZrO$_2$+8 wt.% Y$_2$O$_3$ coatings. *J. Eur. Ceram. Soc.* **2011**, *31*, 2089–2098. [CrossRef]
15. Ganvir, A.; Calinas, R.F.; Markocsan, N.; Curry, N.; Joshi, S. Experimental visualization of microstructure evolution during suspension plasma spraying of thermal barrier coatings. *J. Eur. Ceram. Soc.* **2019**, *39*, 470–481. [CrossRef]
16. Fazilleau, J.; Delbos, C.; Rat, V.; Coudert, J.F.; Fauchais, P.; Pateyron, B. Phenomena involved in suspension plasma spraying part 1: Suspension injection and behavior. *Plasma Chem. Plasma Process.* **2006**, *26*, 371–391. [CrossRef]

17. Carpio, P.; Blochet, Q.; Pateyron, B.; Pawłowski, L.; Salvador, M.D.; Borrell, A.; Sánchez, E. Correlation of thermal conductivity of suspension plasma sprayed yttria stabilized zirconia coatings with some microstructural effects. *Mater. Lett.* **2013**, *107*, 370–373. [CrossRef]
18. Fauchais, P.; Montavon, G.; Lima, R.S.; Marple, B.R. Engineering a new class of thermal spray nano-based microstructures from agglomerated nanostructured particles, suspensions and solutions: An invited review. *J. Phys. D Appl. Phys.* **2011**, *44*. [CrossRef]
19. Ganvir, A.; Curry, N.; Govindarajan, S.; Markocsan, N. Characterization of thermal barrier coatings produced by various thermal spray techniques using solid powder, suspension, and solution precursor feedstock material. *Int. J. Appl. Ceram. Technol.* **2015**, *13*, 324–332. [CrossRef]